JBC RESEARCH ARTICLE

The copper-linked *Escherichia coli* AZY operon: Structure, metal binding, and a possible physiological role in copper delivery

Received for publication, November 17, 2021 Published, Papers in Press, November 23, 2021,
https://doi.org/10.1016/j.jbc.2021.101445

Rose C. Hadley[1], Daniel Zhitnitsky[2], Nurit Livnat-Levanon[2], Gal Masrati[3], Elena Vigonsky[2], Jessica Rose[2], Nir Ben-Tal[3], Amy C. Rosenzweig[1,*], and Oded Lewinson[2,*]

From the [1]Departments of Molecular Biosciences and Chemistry, Northwestern University, Evanston, Illinois, USA; [2]Department of Biochemistry and the Rappaport Institute for Medical Sciences, Faculty of Medicine, The Technion-Israel Institute of Technology, Haifa, Israel; [3]Department of Biochemistry and Molecular Biology, George S. Wise Faculty of Life Sciences, Tel Aviv University, Tel Aviv, Israel

Edited by Joseph Jez

The *Escherichia coli yobA–yebZ–yebY* (AZY) operon encodes the proteins YobA, YebZ, and YebY. YobA and YebZ are homologs of the CopC periplasmic copper-binding protein and the CopD putative copper importer, respectively, whereas YebY belongs to the uncharacterized Domain of Unknown Function 2511 family. Despite numerous studies of *E. coli* copper homeostasis and the existence of the AZY operon in a range of bacteria, the operon's proteins and their functional roles have not been explored. In this study, we present the first biochemical and functional studies of the AZY proteins. Biochemical characterization and structural modeling indicate that YobA binds a single Cu^{2+} ion with high affinity. Bioinformatics analysis shows that YebY is widespread and encoded either in AZY operons or in other genetic contexts unrelated to copper homeostasis. We also determined the 1.8 Å resolution crystal structure of *E. coli* YebY, which closely resembles that of the lantibiotic self-resistance protein MlbQ. Two strictly conserved cysteine residues form a disulfide bond, consistent with the observed periplasmic localization of YebY. Upon treatment with reductants, YebY binds Cu^{+} and Cu^{2+} with low affinity, as demonstrated by metal-binding analysis and tryptophan fluorescence. Finally, genetic manipulations show that the AZY operon is not involved in copper tolerance or antioxidant defense. Instead, YebY and YobA are required for the activity of the copper-related NADH dehydrogenase II. These results are consistent with a potential role of the AZY operon in copper delivery to membrane proteins.

Copper is an essential prokaryotic micronutrient that serves as a cofactor for key enzymes involved in respiration and redox defense such as cytochrome *c* oxidase, NADH dehydrogenase II (NDH-2), and superoxide dismutase (1, 2). However, copper is also toxic if present in high concentrations and/or in the wrong cellular compartments, partly because of copper-mediated generation of free radicals *via* the Fenton reaction and disruption of iron–sulfur clusters (3–6). Therefore, bacteria employ a variety of resistance and regulation mechanisms that allow copper delivery to designated target proteins, while also affording protection from copper overload (2, 6).

Copper resistance mechanisms primarily involve two chromosomally encoded multicomponent systems, Cue (*Cu efflux*) and Cus (*Cu sensing*). The Cue system consists of the periplasmic multicopper oxidase CueO, the membrane-embedded ATP-driven copper efflux pump CopA, and the transcriptional regulator CueR, which upregulates the expression of CueO and CopA in response to elevated copper concentrations (7–9). The Cus system includes the tripartite CusABC complex, which spans the inner membrane, periplasm, and outer membrane. CusABC functions as a proton gradient–driven efflux pump, exporting Cu^{+} either directly from the cytosol or from the periplasm with the aid of the periplasmic protein CusF (10, 11). The Cus system responds to high copper concentrations *via* regulation by the CusRS two-component system (12).

The plasmid-borne Cop/Pco (*cop*per resistance or *p*lasmid-borne *co*pper resistance) genes represent a third major bacterial copper handling system that includes at least six proteins, CopABCDRS (13, 14). Unlike the Cue and Cus systems, the roles of the individual Cop proteins are not well understood. CopB and CopD have been proposed to import copper into the periplasm and cytoplasm, respectively (15), whereas CopA is a periplasmic multicopper oxidase (16) and CopC is a periplasmic copper-binding protein (17) suggested to work in concert with CopD (15). Copper-inducible expression of these proteins is regulated by the CopRS two-component system. While gene disruption studies have linked these operons to copper resistance (14, 18), expression of the CopC and CopD proteins alone confers copper hypersensitivity (15), suggesting an import function. Genes encoding CopC and CopD are found together or as fusions in the genomes of a range of bacteria in the absence of the other *cop* genes present in the Cop/Pco plasmid-encoded resistance

* For correspondence: Amy C. Rosenzweig, amyr@northwestern.edu, Oded Lewinson, lewinson@technion.ac.il.
Present address for Daniel Zhitnitsky: Department of Internal Medicine (Infectious Diseases), Yale University School of Medicine, New Haven, Connecticut, USA.

operons (19–22). One CopCD fusion protein, *Bacillus subtilis* YcnJ, has been implicated in import by genetic disruption studies (20). While pathways of bacterial copper import to the cytoplasm have not been investigated extensively because of the extracytoplasmic localization of most cuproenzymes, recent data suggest that some extracytoplasmic cuproenzymes, such as cytochrome *c* oxidase and periplasmic copper, zinc superoxide dismutase, are metallated by copper that is first imported to the cytoplasm and then exported back to the periplasm (23–26).

Genes encoding CopC and CopD homologs are also found on the *Escherichia coli* chromosome. These proteins are designated YobA (CopC homolog) and YebZ (CopD homolog), and along with a third protein, YebY (Domain of Unknown Function 2511 [DUF2511]) are encoded by the AZY operon (27). Two transcriptional initiation sites homologous to the copper-responsive "copper boxes" of the *pco* resistance operon (28) are present at positions -34 and -22. Notably, unlike the *pco*, *cop*, and *cus* gene clusters, the AZY operon is also regulated by the small noncoding RNA, FnrS. Under anaerobic conditions, FnrS negatively regulates the AZY operon and numerous additional genes mainly involved in respiration and antioxidant defense (29, 30). Given that *E. coli* has been the focus of numerous copper homeostasis studies, it is surprising that the AZY operon proteins have rarely been mentioned in the literature (17, 31). Despite the presence of this operon in many strains of *E. coli* and in other proteobacteria, firmicutes, and actinobacteria, its physiological role and the proteins involved have not been investigated. Here, we present an initial characterization of the YobA–YebZ–YebY system, including bioinformatics analysis of the YebY family, determination of the YobA and YebY metal-binding properties, the high-resolution crystal structure of YebY, and a possible physiological role of the AZY operon. The combined findings provide new insight into the function of this operon.

Results

Model structure and metal-binding properties of YobA

YobA is a member of the CopC family (PF04234) of periplasmic copper-binding proteins. All structurally characterized CopC proteins exhibit a seven-stranded β-barrel fold (17, 32–36). While a small subset of CopC proteins contain distinct Cu^{+}-binding and Cu^{2+}-binding sites, most family members bind a single Cu^{2+} ion. Based on its sequence, YobA belongs to this majority class, in which the Cu^{2+} ion is coordinated by an amino-terminal nitrogen, two histidine side-chain nitrogens, and an aspartic acid (17). In homology models of YobA generated using five different NMR and crystal structures of CopC from four different organisms as templates, residues His27, Asp111, and His113 are well positioned to form the predicted Cu^{2+}-binding site (Fig. S1).

To study metal binding by YobA, we amplified the complete *yobA* gene (including its signal peptide) from the genome of the WT *E. coli* strain BW25113 and inserted it into a pET21 expression plasmid. A stop codon was inserted before the His_6 sequence to avoid possible complications from metal binding to the His_6 tag. Mature YobA (~11 kDa) was purified to homogeneity (Fig. S2) from osmotic shock extracts of cells overexpressing YobA by a combination of ion exchange and gel filtration chromatography, and its identity was verified by MS. We then measured Cu^{2+} binding by isothermal titration calorimetry, which gave a K_A value of $\sim 3.3 \times 10^8$ M^{-1} ($K_D \sim 3 \times 10^{-9}$ M) (Fig. 1*A*). Consistent with the lack of a

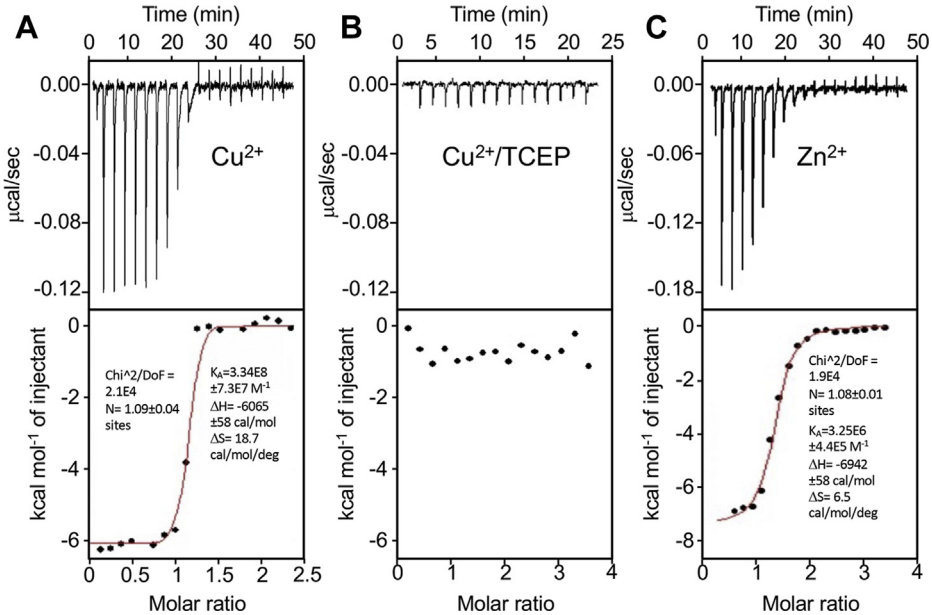

Figure 1. Isothermal titration calorimetry measurements of metal binding by YobA. Shown are the serial injections of 2 µl of (*A*) 0.12 mM $CuSO_4$, (*B*) 0.12 mM $CuSO_4$ + 1 mM TCEP, and (*C*) 0.2 mM $ZnSO_4$ into a 200 µl solution of 12 µM YobA. Results are representative of experiments repeated at least three times. The *upper panels* show the calorimetric titration, and the *lower panels* display the integrated injection heat derived from the titrations, for which the best-fit curve (*red trace*) of a simple 1:1 interaction model was used to calculate the K_A. The K_A values are mean ± STD (standard deviation) of three independent experiments. Also shown are the goodness of the fit (Chi^2/DoF) and the changes in enthalpy (ΔH) and entropy (ΔS) upon binding. TCEP, Tris(2-carboxyethyl)phosphine.

methionine-rich Cu^{+}-binding motif (17), YobA displayed no measurable Cu^{+} binding (Fig. 1*B*). We also measured the binding affinity of YobA for several additional divalent metal ions. We could not detect binding of Mn^{2+}, Cd^{2+}, Fe^{2+}, Pb^{2+}, or Mg^{2+} (Table S1). Binding of Zn^{2+}, Ni^{2+}, Co^{2+}, and Hg^{2+} was observed, albeit with affinities that are two to three orders of magnitude lower than that of YobA for Cu^{2+} (Fig. 1*C* and Table S1). Similar results were obtained in metal-mediated tryptophan fluorescence quenching experiments. The most prominent quench was observed in the presence of Cu^{2+} (Fig. 2*A*), whereas no quench was observed upon addition of Cu^{2+} in the presence of the reducing agent DTT (Fig. 2*B*). Collectively, these results indicate that YobA is a typical Cu^{2+}-binding CopC protein.

Bioinformatics analysis and cellular localization of YebY

Unlike YobA and YebZ, which belong to the known CopC and CopD protein families, respectively (17, 22), YebY belongs to the uncharacterized Protein family 10709 (pfam10709)/DUF2511 protein family (17, 31), and its connection to copper homeostasis is unknown. As such, we conducted a comprehensive bioinformatics analysis of sequences associated with pfam10709 available in the Joint Genome Institute (JGI)/Integrated Microbial Genomes genome database. The majority of YebY sequences are found in Gram-negative bacteria, and specifically in γ-proteobacteria (Fig. 3*A*), most commonly within the Enterobacteriaceae family. Other well-represented families include Erwiniaceae, Yersiniaceae, Morganellaceae, and Pectobacteriaceae. The next most represented class is Actinobacteria, including Bifidobacteriaceae, Microbacteriaceae. Mycobacteriaceae, Nocardiaceae, and Streptosporangiaceae. The *E. coli* K12 YebY investigated here belongs to the largest cluster of sequences, suggesting that it is an appropriate representative of γ-proteobacterial YebY homologs and the broader Pfam10709/DUF2511 family. The only previously studied family member is the putative lantibiotic self-resistance protein MlbQ from the Gram-positive actinomycete *Microbispora* ATCC PTA-5024 (37). Comparisons of YebY and MlbQ will therefore provide useful insight into the similarities and differences between γ-proteobacterial and actinobacterial Pfam10709 members (Fig. 3*A*).

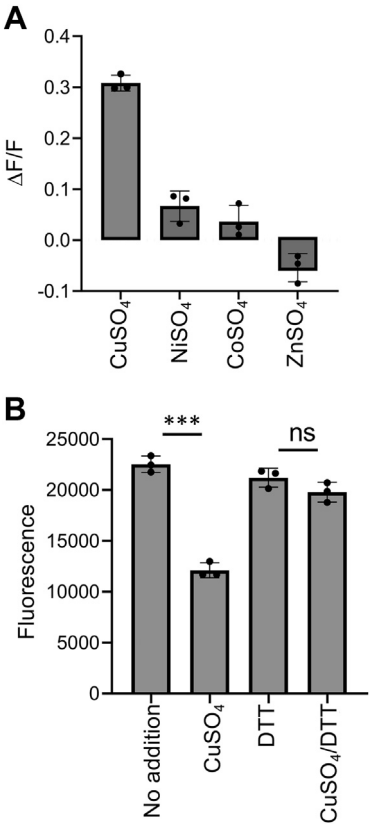

Figure 2. Fluorescence quenching measurements of metal binding by YobA. *A*, the fluorescence (excitation of 280 nm and emission of 325 nm) of 2 μM YobA was measured in the presence of 10 μM $CuSO_4$, $NiSO_4$, $CoSO_4$, and $ZnSO_4$. The fractional quench of fluorescence (ΔF/F) relative to metal-free YobA is shown. The results are the mean ± standard deviation of the mean of triplicates. *B*, the fluorescence intensity (excitation of 280 nm and emission of 325 nm) of 2 μM YobA in the absence or the presence of 10 μM of $CuSO_4$, 1 mM DTT, or 10 μM $CuSO_4$ + 1 mM DTT, as indicated. Normal distribution of the data was verified by the Shapiro–Wilk test ($\alpha = 0.05$), and statistics were calculated using one-way ANOVA. ***$p < 0.005$. ns, not significant.

We assessed the cellular localization of the YebY family by identifying predicted signal sequences using the LipoP 1.0 server (38, 39). The vast majority of analyzed sequences contain a predicted signal peptide, with a minority predicted to harbor lipoprotein signal peptides (Fig. S3). *E. coli* YebY contains a predicted signal peptide, whereas MlbQ contains a lipoprotein signal peptide that may facilitate lipid attachment to Cys36, the first residue after the predicted cleavage site, and subsequent membrane anchoring. The widespread presence of signal peptides indicates that YebY homologs are extracytoplasmic in both Gram-positive and Gram-negative bacteria. To verify the cellular localization of YebY, we cloned the full sequence, including the signal peptide, from *E. coli* BW25113 and inserted it into a pET-derived expression vector harboring a C-terminal His_6 tag. YebY-His_6 was then expressed in the *E. coli* BL21-Gold (DE3) strain, and the cells were fractionated into cytosolic, membrane, and periplasmic compartments. Immunoblotting of SDS-PAGE indicates that YebY localizes exclusively to the periplasm (Fig. S4*A*).

In addition, we performed a genomic neighborhood analysis using representative node sequences to determine how frequently genes encoding YebY family members are encoded in conjunction with *copC* or *copD*-like genes. Approximately 52% of representative genes encoding YebY homologs are found in proximity to both *copC* and *copD* in AZY-like genomic contexts (Fig. 3*B*). Of those genes, >97% exhibit the canonical gene ordering of *yebY* adjacent to *copD* and two genes away from *copC*. Two *E. coli* species harbor YebZ–YebY fusions that are present next to YobA. However, a significant number of genes encoding YebY homologs exist in different genomic contexts. Many homologs are not part of an operon, including members of the Pectobacteriaceae, Micrococcales, Mycobacteriaceae, Erwinia, and Chryseobacteria. In other cases, *yebY* is present in an operon unrelated to copper homeostasis. For example, YebY is encoded between the site-specific recombinase XerD (COG4974) and the bacteriophage

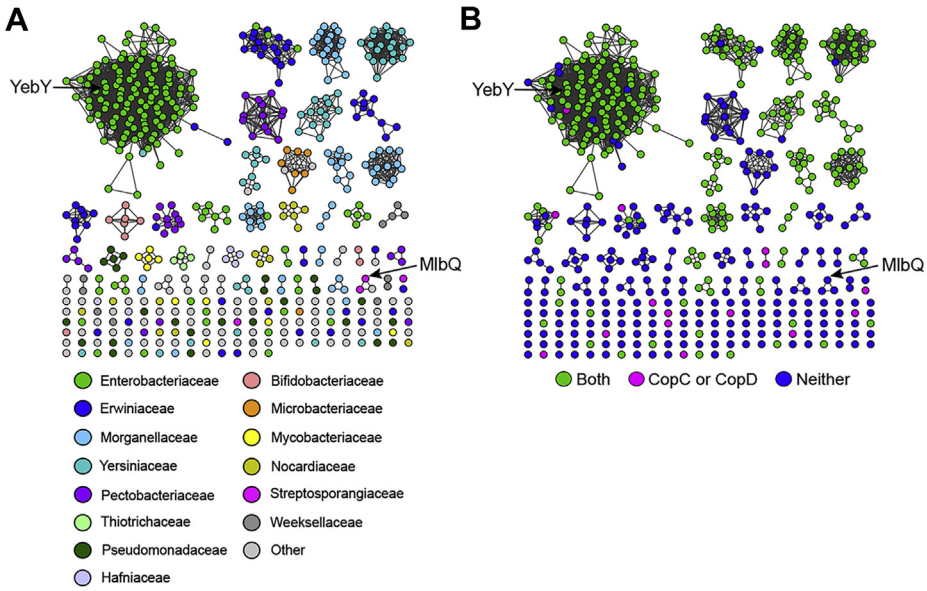

Figure 3. Sequence similarity network of YebY homologs constructed using the EFI/EST sequence similarity network generation tool at an alignment score threshold of 48. Colored by (*A*) bacterial family and (*B*) genomic proximity to CopC and CopD. EFI/EST, Enzyme Function Initiative/Enzyme Similarity Tool.

CI repressor helix–turn–helix domain-containing protein (PF07022) in a number of Enterobacteriaceae. In some Mycobacteriaceae, *yebY* is downstream of a transcriptional regulator (contains XRE-family HTH domain, COG1396). By contrast, the homolog MlbQ is present along with genes encoding ABC transporters in an operon associated with lantibiotic resistance (37).

Biochemistry and structure of YebY

To facilitate biochemical analysis of YebY, we purified it from osmotic shock extracts. To avoid possible complications from metal binding to the tag, we inserted a stop codon before the His_6 sequence. Untagged mature YebY (~11 kDa) was purified to homogeneity from the periplasmic compartment using size-exclusion chromatography (SEC; Fig. S4*B*, *inset*). Inductively coupled plasma MS (ICP–MS) analysis indicated that YebY purifies in the absence of metal ions (Table S2). SEC with multiangle light scattering (SEC–MALS) analysis of purified YebY showed a homogeneous monomer with a molar mass of 11 kDa (Fig. S4*B*). Given the presence of two highly conserved cysteine residues and the periplasmic localization of YebY, we investigated the possibility of a disulfide bond. On SDS-PAGE, the oxidized form of YebY migrates faster than the reduced form, suggesting a more compact conformation of the former (Fig. S5*A*). In addition, reduction of YebY decreased the midpoint temperature for thermal denaturation by ~5 °C, consistent with the presence of a stabilizing disulfide bond (Fig. S5*B*). Moreover, replacement of either Cys48 or Cys113 by site-directed mutagenesis to Ala or Ser completely abrogated protein expression. Collectively, these results indicate that a Cys48–Cys113 disulfide bond is indeed formed.

To gain a molecular-level understanding of YebY, we took advantage of the two methionine residues in YebY and prepared a selenomethionine-labeled analog (SeMet-YebY) for crystallography. SeMet-YebY crystallized readily, and the 1.8 Å resolution structure was solved using Se single-wavelength anomalous dispersion phasing (Table 1). The space group is $P2_1$ with 12 monomers in the asymmetric unit arranged as dimers. The monomer structure comprises an antiparallel four-stranded β sheet surrounded by four α helices. As anticipated, the C-terminal cysteine (Cys113) forms a disulfide bond with a cysteine at the C terminus of the second β-strand (Cys48), stabilizing a compact fold (Fig. 4, *A* and *B*). Alignment of the structure with the NMR structure of the only previously characterized family member, MlbQ (26.9% amino acid

Table 1
Data collection and refinement statistics

	SeMet-YebY
Data collection	
Space group	$P2_1$
Cell dimensions	
a, *b*, *c* (Å)	96.1, 53.2, 132.4
α, *β*, *γ* (°)	90, 102.3, 90
Resolution (Å)	32.79–1.88 (1.95–1.88)
R_{sym}	0.06082 (1.14)
$I/\sigma I$	9.96 (0.61)
Completeness (%)	90.84 (55.27)
Multiplicity	2.0 (2.0)
No. of reflections	193,327 (11,618)
Refinement	
Resolution (Å)	32.79–1.88 (1.95–1.88)
Reflections used in refinement	97,246
R_{work}/R_{free} (%)	23.5/27.0
No. of atoms	
Protein	8659
Water	451
B-factors (Å^2)	
Protein	40.7
Water	43.3
RMSDs	
Bond lengths (Å)	0.031
Bond angles (°)	1.95

Values in parentheses represent the highest-resolution shell.

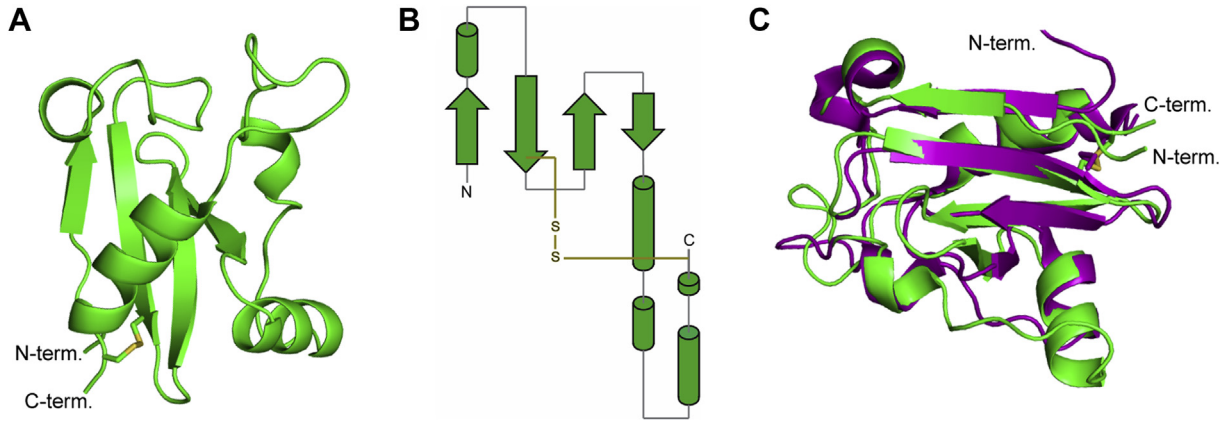

Figure 4. Crystal structure of YebY. *A,* cartoon diagram of YebY. *B,* topology diagram of YebY indicating the location of the disulfide bond. *C,* superposition of YebY (*green*) and MlbQ (Protein Data Bank accession code: 2MVO; *purple*).

identity) (37, 40), reveals a strong similarity with an alignment RMSD of 1.84 Å for 294 atoms and a disulfide bond in the same location (Fig. 4*C*). While there are slight differences in some of the secondary structure elements, the only major difference between the two proteins is the length. The first 58 residues of MlbQ, which include a 34-residue amino-terminal lipoprotein signal peptide, are unstructured (not shown in Fig. 4*C*). The unstructured residues following the signal peptide are presumably a linker between the membrane anchor and the folded domain. In contrast, the first secondary structure element begins at position 25 in the full-length YebY sequence. Thus, the first sequentially and structurally conserved residues are Trp37 (YebY) and Trp71 (MlbQ). The similarity between these two homologs, which are relatively distant within the Pf10709/DUF2511 family, suggests a high degree of structural conservation within the family.

YebY displays low affinity for copper and other metal ions

Given that YebY is encoded in an operon with putative (YebZ) and confirmed (YobA) copper-binding proteins and contains two highly conserved cysteine residues that could bind copper in their reduced state, we investigated its metal-binding properties. YebY lacking the His_6 tag in its native state or treated with the reductant tris(2-carboxyethyl)phosphine (TCEP) was incubated with up to 10 equivalents of Cu^+ or Cu^{2+} in an anaerobic chamber. CD spectra confirm that reduction of the disulfide does not cause a significant change in secondary structure (Fig. S6). Following incubation for ~2 h, unbound copper was removed by desalting. The copper and protein concentrations were then measured by ICP–MS and absorbance at 280 nm, respectively. Without treating YebY with TCEP, very little binding was observed for either Cu^+ or Cu^{2+} (Fig. 5*A*). However, the TCEP-treated (reduced) protein showed measurable binding of both Cu^+ and Cu^{2+}, with a seeming preference toward the former: at a molar ratio of 2:1, ~30% of YebY was occupied by Cu^+, whereas five equivalents of Cu^{2+} were required to reach the same occupancy (Fig. 5*A*). To estimate the binding affinity of reduced YebY for Cu^+, we measured the quenching of intrinsic tryptophan fluorescence and observed a dose-dependent response with a K_D of 50 to 100 μM (Fig. 5*B*). These ICP–MS and

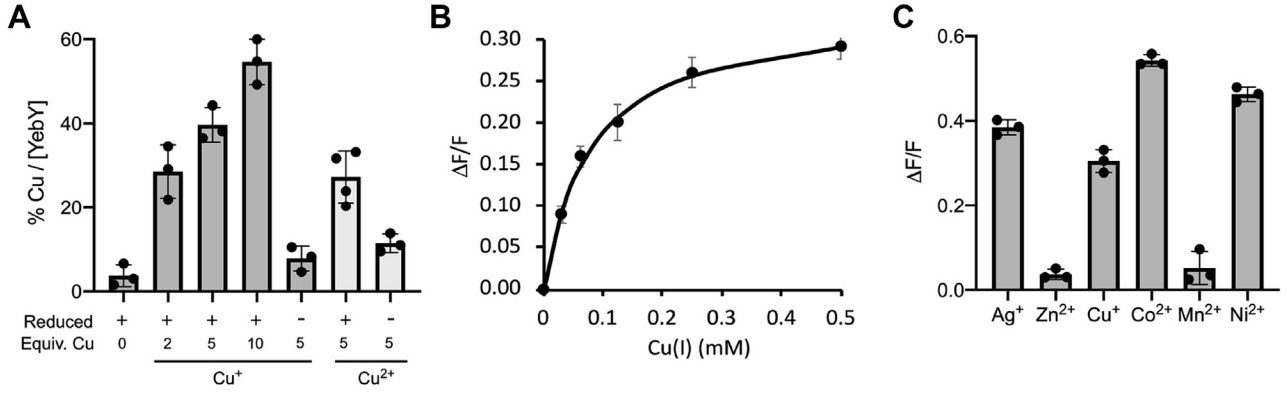

Figure 5. Metal-binding properties of YebY. *A,* YebY (32–56 μM) with (+) or without (–) pretreatment with reductant was incubated with the indicated molar equivalents of Cu^+ or Cu^{2+} under anaerobic conditions. Unbound material was removed by desalting, and the amount of YebY-bound copper was measured by ICP–MS. *B,* YebY (5 μM) was incubated in the presence of 1 mM DTT with the indicated concentrations of Cu^+. The change in fluorescence emission at 340 nm was measured following excitation in 280 nm. *C,* YebY (2.5 μM) was incubated in the presence of 1 mM DTT and 250 μM of the indicated metals. The change in fluorescence emission at 340 nm was measured following excitation at 280 nm. Results shown in (*A–C*) are means of at least three repeats ± standard deviation of the mean. ICP–MS, inductively coupled plasma MS.

tryptophan fluorescence results suggest that the two cysteine residues involved in the disulfide bond can bind Cu^{+} with low affinity.

Quenching of intrinsic tryptophan fluorescence was also used to evaluate the possibility that YebY interacts with other metal ions. A strong quench of fluorescence was observed in the presence of Co^{2+}, Ni^{2+}, and Ag^{+}, whereas a negligible quench was observed in the presence of either Zn^{2+} or Mn^{2+} (Fig. 5*C*). Therefore, unlike YobA, which is a highly specific high-affinity Cu^{2+}-binding protein, YebY seems to bind metal with low affinity and specificity, bringing into question the physiological relevance of YebY as a copper-binding protein, and suggesting that it may play a different role in the AZY operon.

A possible physiological role for the AZY operon

To probe the physiological role of the AZY operon, we constructed *E. coli* strains harboring single deletions of *yobA*, *yebZ*, or *yebY* or a triple *AZY* knockout and compared the susceptibility of WT and deletion strains to various stressors. First, we tested for a role in copper tolerance, since periplasmic copper-binding proteins have been proposed to contribute to copper tolerance (41, 42). However, the WT and *ΔAZY* strains exhibited similar growth over a broad range of copper concentrations (0–2 mM) (Figs. 6*A* and S7). Because of the redundancy of bacterial copper resistance mechanisms, the distinction between tolerant and sensitive phenotypes often requires the use of hypersensitive strains in combination with overexpression of the rescuing protein (43). We therefore overexpressed the individual genes or the entire operon in the background of the copper-sensitive *E. coli* strain GG44, which lacks the copper P_{1B}-ATPase efflux pump CopA (43, 44). As shown in Figure 6*B*, the overexpressed AYZ proteins could not rescue this copper-sensitive strain. These combined results argue against a role for the AZY operon in copper tolerance.

In addition to copper, the *AZY* operon is regulated by the small noncoding RNA, FnrS, which is known to regulate genes involved in antioxidant defense (29, 30). We therefore investigated the possibility that the operon is involved in antioxidant defense. When challenged with the oxidizing agents, hydrogen peroxide (Fig. 6*C*) or paraquat (Fig. 6*D*), the *ΔAZY* strain grew very similarly to the WT strain, suggesting that the *AZY* operon does not play a major role in antioxidant defense.

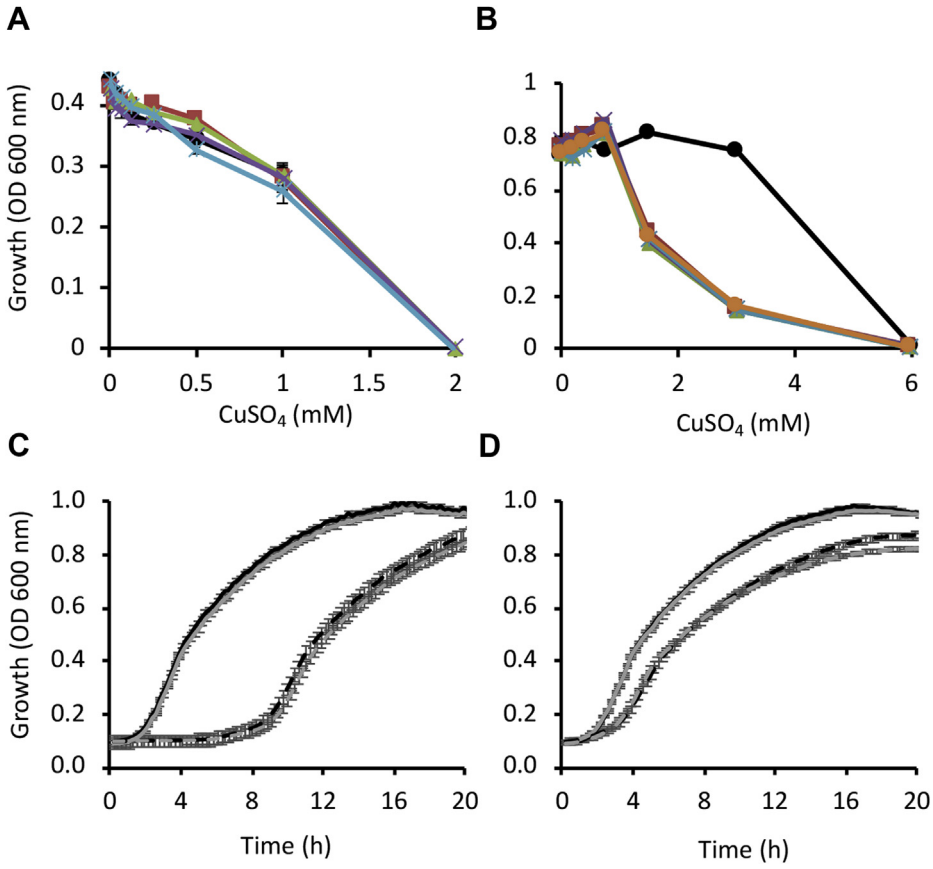

Figure 6. The AYZ operon is not involved in copper tolerance or antioxidant defense. *A,* cultures of WT (*black*), Δ*yobA* (*red*), Δ*yebY* (*green*), Δ*yebZ* (*blue*), or Δ*AYZ* (*purple*) *Escherichia coli* were grown for 12 h in Davis minimal media in the presence of 0 to 2 mM $CuSO_4$, as indicated. *B,* cultures of WT *E. coli* (*black*) or the copper-sensitive GG44 strain (*all other curves*) were grown for 12 h LB media in the presence of 0.1 mM IPTG and 0 to 2 mM $CuSO_4$, as indicated. The GG44 cells were transformed with an empty control vector (*orange*) or with plasmids for the overexpression of YobA (*red*), YebY (*green*), YebZ (*blue*), or AYZ (*purple*). *C,* cultures of WT (*black*) or Δ*AYZ* (*gray*) *E. coli* were grown in LB media for the indicated times in the absence (*solid traces*) or the presence (*dashed traces*) of 0.0025% hydrogen peroxide. *D,* cultures of WT (*black*) or Δ*AYZ* (*gray*) *E. coli* were grown in LB media for the indicated times in the absence (*solid traces*) or the presence (*dashed traces*) of 0.25 mM paraquat. Results shown in (*A–D*) are means of at least three repeats, and error bars (shown unless smaller than the icons) represent ± standard deviation of the mean.

Taking into account the copper-binding capacity of YobA and the periplasmic localization of YobA and YebY, another possibility is that the operon functions in copper delivery to membrane-embedded copper proteins. Such a role has been demonstrated for two periplasmic copper chaperones of the purple photosynthetic bacteria *Rhodobacter capsulatus* (45). To probe for copper content of membrane proteins, we isolated membranes from early exponential-phase cultures of WT and *ΔAZY* cells and monitored the activity of NADH-NDH-2. This membrane-embedded enzyme catalyzes the transfer of electrons from NADH to its copper cofactor or to copper cofactors of other membrane proteins (46–48). The activity of NDH-2 therefore provides a proxy for the amount of membrane-bound copper.

In buffered solution (in the absence of membranes), NADH is stable, and its oxidation is not observed on the timescale of the experiment (Fig. 7, *black trace*). Addition of the WT *E. coli* membrane fraction greatly accelerated the rate of NADH oxidation (Fig. 7, *red trace*). The oxidation rate of NADH in the presence of membranes prepared from cells lacking NDH-2 (*Δndh*) was nearly identical to that observed in buffer (Fig. 7, *green trace*), corroborating previous reports that in such early exponential-phase cultures, NDH-2 is the main NADH oxidase (49, 50). Relative to WT membranes, membranes prepared from the *ΔAZY* cells displayed significantly reduced NADH oxidation activity (Fig. 7, *blue trace*), despite containing WT-like levels of NDH-2 as determined by LC–MS^2 proteomic comparison of WT and *ΔAZY* cells (Fig. S8). These results imply that the AZY operon contributes to copper delivery to NDH-2 and/or to other membrane proteins. We then prepared membranes from strains carrying single deletions of *yobA*, *yebZ*, *or yebY*. The *ΔyebZ* membranes displayed the same NADH oxidation activity as the WT membranes (Fig. 7, *cyan trace*). Of the two remaining genes, the deletion of *yobA* more strongly affected the NADH oxidation activity compared with the deletion of *yebY* (Fig. 7, compare *purple* and *orange curves*), and the combined effects of the single deletions *ΔyobA* and *ΔyebY* accounted for the effect observed upon deletion of the entire operon. Importantly, transformation of the *ΔyobA* and *ΔAZY* strains with plasmids encoding the deleted genes restored the NADH oxidation activity to WT levels (Fig. S9). Collectively, these results suggest that YebZ is dispensable for NDH-2 activity, whereas YobA and YebY contribute to it.

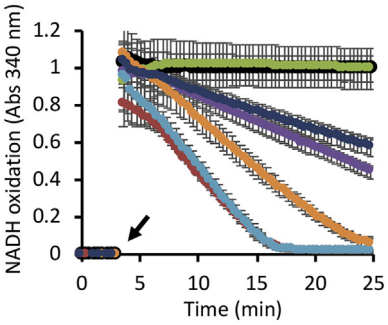

Figure 7. YobA and YebY contribute to the activity of NDH-2. At the time indicated by the *arrow* (~3 min), 1 mM NADH was injected into buffered solution in the absence (*black trace*) or the presence (*all other traces*) of membrane fractions (1 mg/ml) prepared from early exponential phase cultures of WT *Escherichia coli* (*red*), *Δndh* cells (*green*), *ΔAZY* (*blue*), *ΔyebZ* (*cyan*), *ΔyobA* (*purple*), or *ΔyebY* (*orange*). The rate of NADH oxidation was monitored by measuring the absorbance at 340 nm. Results shown are means of triplicates ± standard deviation of the mean. NDH-2, NADH dehydrogenase II.

Discussion

The *E. coli* AZY operon encodes two periplasmic proteins, YobA and YebY, and a third uncharacterized membrane protein, YebZ, which belongs to the CopD family of putative copper importers. While genes encoding YobA and YebZ homologs are typically found together or as fusions (19–22), our bioinformatics analysis shows that YebY is frequently found in other genomic contexts, perhaps suggesting distinct roles within and beyond the AZY operon. YobA contains the canonical His–Asp–His C_{0-2} Cu^{2+}-binding site (17), and as expected, displays high specificity and affinity for Cu^{2+} (K_D ~ 3 nM). In contrast, YebY is more promiscuous and binds several metals (including Cu^{2+} and Cu^{+}) with low affinity (K_D = 50–100 μM). Metal binding by YebY is enhanced following reduction of the protein, suggesting that the two highly conserved cysteines of YebY can participate in metal coordination. However, the low affinity of copper binding by YebY along with the stabilization imparted by the disulfide suggests that this metal binding is likely not physiologically relevant.

Genetic disruptions indicate that the AZY operon is not involved in copper tolerance or antioxidant defense but instead point to a possible role in copper delivery to membrane targets. It is intriguing that despite the fourfold to fivefold difference in copper-binding affinities between YobA and YebY, both seem to be required for full activity of the copper-dependent NDH-2. Given the striking structural similarity between YebY and MlbQ, the function of YebY may also be related to that of MlbQ. Resistance to the self-produced lantibiotic NAI-107 in *Microbispora* ATCC PTA-5024 is proposed to derive from direct binding of NAI-107 to MlbQ (37). Notably, copper has been previously linked to antibiotic resistance in *E. coli* (51). Further investigation of the role of the AZY operon in copper delivery and potentially antibiotic resistance represents an important future direction.

Despite their broad distribution and extensive structural and biochemical characterization, the roles of YobA family members have remained surprisingly elusive (13, 17, 34, 45, 52). Even less is known about YebZ homologs (CopD family), and YebY proteins were characterized here for the first time, despite the presence of the AZY operon in *E. coli*. By contrast, the roles of the copper-detoxifying systems, Cue and Cus, are fairly well established (53, 54). One possible explanation for this dichotomy in knowledge may lie in the universality of copper toxicity and copper tolerance mechanisms *versus* the divergence of copper utilization. The challenge of copper toxicity is faced by all bacteria, and the main defense mechanisms appear to have been highly conserved throughout evolution. Copper utilization, on the other hand, is less universal:

only a handful of copper-dependent/containing proteins are present in each bacterium, and this subset varies between different bacteria (2). Moreover, in some bacteria, copper is needed in compartments or metabolic pathways that do not exist in other bacteria (*e.g.*, thylakoids of cyanobacteria (55), intracytoplasmic membranes of methanotrophic bacteria (56), reduction of N_2O by denitrifying bacteria (57)). These specialized needs likely led to divergence of the utilization/delivery pathways, rendering the assignment of physiological roles difficult. In *E. coli*, and perhaps in other enterobacteria, we suggest that the *AZY* system is not involved in copper tolerance or import but rather in its delivery to specific membranal targets.

Experimental procedures

Homology modeling of YobA

Template structures were collected using the Hidden Markov model (HMM)-based homology detection algorithm HHpred (58). Five CopC NMR and crystal structures from four different organisms were identified as potential templates for modeling. These included the crystal structures of CopC from *E. coli* (Protein Data Bank [PDB]: 1LYQ; 46% sequence identity), *Pseudomonas syringae* (PDB: 2C9Q; 39% sequence identity), *Methylosinus trichosporium* OB3b (PDB: 5ICU; 29% sequence identity), and *Pseudomonas fluorescens* (PDB: 6NFR; 37% sequence identity), and an NMR structure of CopC from *P. fluorescens* (PDB: 6TPB). For YobA and each of the templates, sequences of homologs were collected using HMMER (59) against the Clean-UniProt database with a maximal sequence identity of 95% and a minimal sequence identity of 35%. These sequences were then aligned using MAFFT (60) to produce multiple sequence alignments (MSAs). Next, each of the template MSAs was aligned to the MSA of YobA using HHalign (61). Pairwise alignments between the sequences of YobAs and each of the templates were deduced from these profile-to-profile MSAs.

For each of the five templates, MODELLER-9.18 (62) was used with default parameters to produce 100 models of YobA. A short steepest descent energy minimization was then carried out for each model using GROMACS-2019 (63) and the AMBER99SB-ILDN force field (64). The model with the lowest predicted energy was selected for further analysis. Finally, the MSA of YobA was used with the ConSurf Web server (65) to calculate the conservation scores of amino acids that were mapped onto the 3D model. Overall, the YobA model is consistent with the expected evolutionary pattern, in which the core of the protein is highly conserved and the periphery more variable. One exception is a highly conserved patch on the protein's surface, consisting, among others, of amino acids His 27, Asp 111, and His 113. Importantly, the equivalent residues in the *P. fluorescens* CopC crystal structure bind Cu^{2+} ions (36).

Cloning, expression, and protein purification

The *yobA* and *yebY* genes were PCR amplified from the parental strain of the Keio collection (66) (*E. coli* strain BW25113) and inserted into a pET-21b (Novagen) expression vector carrying a His_6 C-terminal affinity tag. The His_6 tag was used for preparation of YebY for crystallization. For all metal-binding assays, tag-free variants of YebY and YobA were prepared by inserting a stop codon before the His_6 coding region. YebY and YobA were expressed in *E. coli* BL21-Gold (DE3) cells grown at 37 °C in either LB or terrific broth glycerol supplemented with 100 μg/ml ampicillin. To induce protein expression, 1 mM IPTG was added to midexponential phase cultures for 2 to 4 h. Cells were then harvested by centrifugation for 20 min at 8000*g* and stored at −80 °C. Periplasmic extracts were prepared by osmotic shock: cell pellets were resuspended (10 ml/1 g cells) in 40% sucrose, 1 mM EDTA, 10 mM Tris–HCl, pH 7.5, and agitated gently at 4 °C for 1 to 3 h, followed by 5 to 15 min agitation at room temperature. The cells were then squirted into 100-fold excess volume milliliters of ice-cold 0.5 to 250 mM EDTA, pH 8, and stirred vigorously for 5 min. Prior to centrifugation at 8000*g* for 30 min, 50 mM Tris–HCl, pH 7.5, 250 mM NaCl, 30 μg/ml DNase (Worthington), 1 EDTA-free protease inhibitor cocktail tablet (Roche) (or 1 mM PMSF), and 1 to 2 mM $MgCl_2$ were added to the cell suspension. Because of the high periplasmic content of YobA or YebY, this step alone yielded 50 to 80% purity. Tag-free YobA and YebY were further purified by SEC using a HiLoad 16/600 Superdex 75 or 200 column (GE Healthcare) using 50 mM Tris–HCl, pH 7.5, 250 mM NaCl. Fractions were analyzed by SDS-PAGE, pooled, and concentrated to ∼10 to 20 mg/ml using Amicon Ultra concentrators (Millipore) with a molecular cutoff of 8 to 10 kDa.

Selenomethionine-labeled His_6-tagged YebY was purified as described for native YebY, with the following modifications. Osmotic shock was performed using 40% sucrose, 1 mM EDTA, 10 mM Tris, pH 8.0 followed by addition of 2 mM $MgCl_2$, 20 mM imidazole, 1 mM PMSF, 20 mM Tris–HCl, pH 8.0, and 250 mM NaCl. The protein was purified using a 5 ml Ni-loaded HisTrap column by elution with imidazole. Imidazole was then removed using a HiPrep 26/10 column equilibrated with 50 mM Tris–HCl, pH 7.5, 250 mM NaCl, and the protein was incubated with 10 mM EDTA for 1 h followed by two cycles of dialysis against 50 mM Tris–HCl, pH 7.5, 250 mM NaCl, 1 mM TCEP, once for 3 h and again overnight.

Isothermal titration calorimetry of YobA

Calorimetric measurements were performed with a MicroCal iTC200 System (GE Healthcare). Prior to the experiment, YobA was dialyzed extensively against 25 mM Tris–HCl, pH 8, 150 mM NaCl. To reduce buffer incompatibility, metal stocks were prepared in this dialysis buffer. All measurements were carried out at 25 °C. Aliquots (2 μl) of metal in the indicated concentrations were added by a rotating syringe to the reaction chamber containing 200 μl of 12 μM YobA. Cu^{2+} was added as $CuSO_4$, and Cu^{+} was added as $CuSO_4$ + 1 mM TCEP. Data fitting was performed with ORIGIN 7.0 assuming a simple 1:1 binding model in which the metal-free form of the protein is in equilibrium with the metal-bound species.

Bioinformatics of YebY

YebY belongs to the DUF2511 family and is part of Pfam10709. All sequences corresponding to Pfam10709 (12,376) were downloaded from JGI/Integrated Microbial Genomes on April 13, 2020. A sequence similarity network was created using the EFI-EST web tool (67) with an *E*-value cutoff of 5. Representative nodes were created using a 100% sequence identity cutoff, resulting in 1224 unique amino acid sequences. These sequences were then aligned against the HMM for Pfam10709 using HMMalign (68) and visualized in Jalview (69). The vast majority of the downloaded sequences contained two highly conserved cysteine residues, so truncated sequences lacking one or both cysteine residues were removed from the dataset. A sequence similarity network was then created using the EFI-EST web tool (67) with an *E*-value cutoff of 5. Representative nodes were created using a 95% sequence identity cutoff, resulting in 539 unique amino acid sequences. The resulting network was visualized using Cytoscape 3.7.2 (70). Metadata from JGI were added for each representative node gene to visualize on the network, including the family of each representative node sequence. The LipoP 1.0 server was used to predict whether each representative sequence contains a signal peptide or lipoprotein signal peptide (38). In addition, the genomic neighborhoods and the proximity of PF10709 to CopC (PF04234) and CopD (PF05425) genes were assessed by evaluating five genes upstream and downstream of YebY.

SEC–MALS

SEC–MALS was used to determine the oligomeric state of untagged YebY. Aliquots of YebY were thawed and buffer exchanged using 10 kDa MWCO (molecular weight cutoff) concentrators (Millipore) into 20 mM Hepes, pH 7.0, 100 mM NaCl. Samples (250 μl, ∼300 μM) were prepared at room temperature immediately before use and analyzed using an Agilent 1260 series HPLC system equipped with diode array detection absorbance in-line with a DAWN HELEOS II multiangle static light scattering detector (Wyatt Technology), a QELS dynamic light scattering detector (Wyatt Technology), and a T-rEx differential refractive index detector (Wyatt Technology). The samples were injected onto a Superdex 75 Increase 10/300 GL column (GE Healthcare) that had been pre-equilibrated in running buffer (20 mM Hepes, pH 7.0, 100 mM NaCl). The buffer was stored at room temperature, and the column was kept at 8 °C. Each sample was run at 0.4 ml min^{-1} for 60 min. Data processing and analysis were performed using Astra software, version 5.3.4 (Wyatt Technology).

Crystallization and structure determination

Selenomethionine-labeled His_6-tagged YebY was prepared to facilitate structure determination. YebY was transformed into the methionine-auxotrophic strain B834(DE3). About 5 ml of starter cultures were grown overnight at 37 °C with shaking in total M9 medium supplemented with 0.4% glucose, 2 mM magnesium sulfate, 0.1 mM calcium chloride, 25 μM ferric sulfate (or 40 μM ferric citrate), 100 μg/ml ampicillin, and 50 μg/ml methionine. The starter culture was used to inoculate 1 l of the same media to a starting absorbance of 0.05 to 0.1 at 600 nm. The culture was grown to an absorbance of 1 at 600 nm before it was centrifuged (10 min, 5500*g*, 25 °C). The supernatant was decanted, and the pellet was resuspended in the same media but with omission of methionine. Following 4 to 8 h shaking at 37 °C, selenomethionine was added to a concentration of 50 μg/ml. After 30 min, expression was induced with 0.5 mM IPTG, and the culture was grown overnight at 25 °C. The cells were pelleted by centrifugation (8500*g*, 30 min, 4 °C), flash frozen in liquid nitrogen, and stored at −80 °C until use.

Selenomethionine-labeled His_6-tagged YebY was crystallized by sitting drop vapor diffusion at room temperature by mixing 0.5 μl of 14.2 mg/ml SeMet-YebY with 0.5 μl of well solution containing 0.2 M ammonium sulfate, 0.1 M bis–Tris–HCl (pH 6.5), and 25% (w/v) PEG 3350. Rod-shaped crystals grew within 2 weeks. Crystals were cryoprotected in a solution containing 40% PEG 400 and flash frozen in liquid nitrogen. Diffraction data were collected at LS-CAT Sector 21 of the Advanced Photon Source at Argonne National Laboratory at a wavelength of 0.9786 Å. XDS was used to index, integrate, and scale the data (71).The crystals belong to space group $P2_1$, and there are 12 monomers in the asymmetric unit. The structure was solved by single-wavelength anomalous dispersion using phenix.autosol (72). Phenix.autobuild (73) was used to obtain an initial model with an R/R_{free} of 27.6%/31.8%. This model was improved through iterative rounds of model building using Coot (74) and refinement using phenix.refine (75) resulting in a final R/R_{free} value of 23.5%/28.2% (Table 1). The final model includes 1112 residues in 12 chains and 451 water molecules. The Ramachandran plot indicates that 97.1% of residues are in favored regions with 2.57% in allowed regions and the remaining 0.09% are outliers. The Molprobity (76) score is 1.74 (85th percentile).

Metal-binding analysis of YebY

The copper-binding assays were performed under inert atmosphere in a Coy anaerobic chamber. The buffer (20 mM Hepes, pH 7.0, 100 mM NaCl) was degassed on a vacuum line with three rounds of pumping followed by purging with nitrogen with continuous stirring. The buffer was then closed to the atmosphere and brought into the glove box, where the cap was removed and it was stirred for 2 days. Aliquots (50 μl) of YebY were thawed, and ∼2.6 molar equivalents of TCEP were added to YebY from a freezer stock (1 M TCEP dissolved in MilliQ water). The samples were brought into the glove box and incubated with TCEP for ∼1 h. The samples were then applied to a PD-10 desalting column and eluted using 20 mM Hepes, pH 7.0, 100 mM NaCl according to the manufacturer's instructions. The eluted YebY was aliquoted into microcentrifuge tubes; each aliquot contained 4×10^{-8} mols. Tetrakis(acetonitrile)copper(I) hexafluorophosphate (stored in the anaerobic chamber) was freshly dissolved in anhydrous dimethyl sulfoxide (stored in the anaerobic chamber) to ∼50 mM copper concentration, and Cu^+ was added to YebY

(0, 1, 2, 5, or 10 molar equivalent; <0.6% dimethyl sulfoxide per sample). Alternatively, Cu^{2+} was added from a 50 mM stock of $CuCl_2$. The samples were gently inverted to mix thoroughly and incubated for ~2 h before YebY was separated from unbound Cu^{+} using a PD-10 column following the manufacturer's instructions. YebY was eluted with 3 ml of buffer (instead of 3.5 ml to avoid coelution with unbound copper) and collected in 15-ml metal-free polypropylene tubes. The samples were gently mixed by inversion, and the protein concentration was measured using absrbance at 280 nm ($\varepsilon_{oxidized}$ = 8605 M^{-1} cm^{-1}, $\varepsilon_{reduced}$ = 8480 M^{-1} cm^{-1} used for YebY treated with TCEP). The absorbance of each sample was ~0.1 a.u. in a pathlength cuvette of 1 cm. The metal content of the samples was measured by ICP–MS using a Thermo iCAP Q Inductively Coupled Plasma Mass Spectrometer equipped with a CETAC ASX260 autosampler in the Quantitative Bioelement Imaging Center core facility at Northwestern University. ICP–MS samples were prepared by combining 0.5 ml of YebY sample, 9 ml of MilliQ water, and 0.5 ml of concentrated nitric acid (TraceSelect). Standard curves were prepared from a dilution series of a multielement standard (Inorganic Ventures).

CD spectroscopy

A Jasco J-815 CD instrument housed in the Keck Biophysics Facility at Northwestern University was used for all measurements. Proteins were buffer-exchanged into CD buffer (1 mM Tris–HCl, ±TCEP, pH 7.5). Each sample (20 μM protein, 300 μl) was transferred to a quartz cuvette (1 mm path length). Spectra were recorded from 190 to 280 nm using continuous scan mode (50 nm/min) and 2 nm bandwidth. All data represent averages of two replicate baseline-subtracted scans, where the baseline was obtained from a sample of CD buffer.

Tryptophan fluorescence quenching experiments

Purified untagged YebY or YobA was dialyzed against 20 mM Tris, pH 7.5, 150 mM NaCl, and 10 mM EDTA for 4 h to remove any metals remaining in the preparation, and then against three rounds of 20 mM Hepes, pH 7.0, and 150 mM NaCl to wash away the EDTA. The proteins were diluted to 2.5 μM in 20 mM Pipes, pH 7.5, 150 mM NaCl, and metals were added as indicated. Cu^{2+} was added as $CuSO_4$, and Cu^{+} was added as $CuSO_4$ + 1 mM DTT. Where specified, 1 mM DTT was added to both metal and YebY before mixing. Triplicates of 100 μl were measured using a monochromator-based Tecan M200 plate reader (excitation of 280 nm and emission of 320 nm).

Growth experiments

Overnight cultures were diluted to an absorbance of 0.05 at 600 nm, and 150 μl aliquots were grown in 96-well plates in a Tecan Infinite Pro microplate reader. Cultures were grown in LB or in Davis minimal media (as indicated) in the absence or the presence of the indicated concentrations of $CuSO_4$, H_2O_2, or paraquat. Cells were grown with intermittent agitation (30 s on, 2 min off) for 16 h.

Construction of knockout strains

The single-gene deletion strains *ΔyobA*, *ΔyebZ*, and *ΔyebY* were obtained from the *E. coli* genetic stock center at Yale University. The triple knockout (*ΔyobA/ΔyebZ/ΔyebY*, *i.e.*, *ΔAZY)* was generated using the lambda Red recombinase system as described previously (77).

NDH-2 activity assay

Early exponential phase cultures (absorbance at 600 nm ≤0.1) grown in LB at 37 °C were harvested by centrifugation (20 min, 8000*g*, 4 °C) and resuspended in 50 mM Tris–HCl, pH 8, 150 mM NaCl, and 1 mM PMSF. Cells were disrupted using a tip sonicator, and debris was removed by centrifugation at 17,000*g*. Membranes were collected by ultracentrifugation at 150,000*g* for 1 h, washed once with 50 mM Tris–HCl, pH 7.5, resuspended in the same buffer + 10% glycerol (w/v), frozen in liquid nitrogen, and stored in −80 °C. Membranes were thawed on ice and diluted to 1 mg/ml with 50 mM Tris–HCl, pH 7.5, and 90 μl were dispensed in triplicates to a 96-well plate, and the assay was initiated by injection of NADH to a final concentration of 1 mM.

MS analysis

Three colonies each from *E. coli* WT strain BW25113 and the *ΔAZY* strain were grown overnight in M9 minimal media supplemented with 0.5% glucose, 1% thiamine, 1 mM $MgSO_4$, 10 μM $CaCl_2$, and 0.025% arginine and lysine. Cultures were then diluted and grown to early log phase (absorbance at 600 nm ~0.15). Cells were washed with PBS, flash frozen, and stored at −80 °C. Samples were dissolved in 10 mM DTT, 100 mM Tris–HCl, pH 7.5, and 5% SDS, sonicated and boiled at 95 °C for 5 min, and precipitated in 80% acetone. The protein pellets were dissolved in 9 M urea and 400 mM ammonium bicarbonate, reduced with 3 mM DTT (60 °C for 30 min), modified with 10 mM iodoacetamide in 100 mM ammonium bicarbonate (room temperature, 30 min in the dark), and digested in 2 M urea, 25 mM ammonium bicarbonate with modified trypsin (Promega) overnight at 37 °C in a 1:50 (M/M) enzyme-to-substrate ratio. The tryptic peptides were desalted using C18 tips (Top tip, Glygen), dried, and resuspended in 0.1% formic acid.

The peptides were resolved by reverse-phase chromatography on 0.075 × 180 mm fused silica capillaries (J&W) packed with ReproSil reversed phase material (Dr Maisch GmbH). The peptides were eluted with a linear 180 min gradient of 5 to 28%, a 15 min gradient of 28 to 95%, and 25 min gradient at 95% acetonitrile with 0.1% formic acid in water at flow rates of 0.15 μl/min. MS was performed by Q Exactive HFX mass spectrometer (Thermo) in a positive mode (*m/z* 300–1800, resolution 120,000 for MS1 and 15,000 for MS2) using repetitively full MS scan followed by collision-induced dissociation (higher energy collisional dissociation at 27 normalized collision energy) of the 30 most dominant ions (>1 charges) selected from the first MS scan. The automatic gain control settings were 3 × 106 for the full MS and 1 × 105 for the MS/MS scans. The intensity threshold for triggering MS/MS

analysis was 1 × 104. A dynamic exclusion list was enabled with exclusion duration of 20 s.

The MS data were analyzed with the MaxQuant software, version 1.5.2.8 for peak picking and identification using the Andromeda search engine, searching against the *E. coli* proteome from the UniProt database with mass tolerance of 6 ppm for the precursor masses and 20 ppm for the fragment ions. Oxidation of methionine and protein N terminus acetylation were accepted as variable modifications, and carbamidomethyl on cysteine was accepted as static modifications. The minimal peptide length was set to six amino acids, and a maximum of two miscleavages was allowed. The data were quantified by label-free analysis using the same software. Peptide- and protein-level false discovery rates were filtered to 1% using the target-decoy strategy. Protein tables were filtered to eliminate the identifications from the reverse database, common contaminants, and single-peptide identifications.

Data availability

The coordinates and structure factors for *E. coli* YebY have been deposited in the PDB with accession code 7N0J. All other data are contained within the article and supporting information. Raw data are available from the corresponding authors upon request.

Supporting information—This article contains supporting information.

Acknowledgments—Research in the Lewinson laboratory is supported in part by the Rappaport Institute for Biomedical research. Proteomic LC–MS–MS analysis was performed at the Smoler Proteomics Center, Technion, Israel. ICP–MS analysis was performed at the Quantitative Bio-element Imaging Center at Northwestern University, supported by NASA Ames Research Center grant NNA04CC36G, or at the Fredy & Nadine Herrmann Institute of Earth Sciences at the Hebrew University in Jerusalem. SEC–MALS analysis was performed by the Northwestern Keck Biophysics Facility. The LS-CAT beamlines of the Advanced Photon Source are supported by a US DOE Office of Science User Facility operated for the DOE Office of Science by Argonne National Laboratory under contract DE-AC02-06CH11356. We thank Zdzislaw Wawrzak for assistance with crystallographic data analysis.

Author contributions—R. C. H, N. L.-L., G. M., D. Z., E. V., J. R., N. B.-T., A. C. R., and O. L. conceptualization; R. C. H., N. L.-L., G. M., D. Z., E. V., and J. R. investigation; R. C. H., N. L.-L., A. C. R., and O. L. writing–original draft; R. C. H., D. Z., N. L.-L., G. M., E. V., J .R., N. B.-T., A. C. R., and O. L. writing–review and editing; N. B.-T., A. C. R., and O. L. supervision; N. B.-T., A. C. R., and O. L. funding acquisition.

Funding and additional information—This work was supported by the National Science Foundation and Israel Binational Science Foundation Molecular and Cellular Biosciences grant 1938715 (to A. C. R., O. L., and N. B.-T.) and US Department of Energy (DOE) Basic Energy Sciences grant DE-SC0016284 (to A. C. R.). The research of N. B.-T. is supported in part by the Abraham E. Kazan Chair in Structural Biology, Tel Aviv University.

Conflict of interest—The authors declare that they have no conflicts of interest with the contents of this article.

Abbreviations—The abbreviations used are: AZY, *yobA–yebZ–yebY*; Cop/Pco, *cop*per resistance or *p*lasmid-borne *co*pper resistance; Cue, *Cu* efflux; Cus, *Cu* sensing; DOE, Department of Energy; DUF2511, Domain of Unknown Function 2511; HMM, Hidden Markov model; ICP–MS, inductively coupled plasma MS; JGI, Joint Genome Institute; MSA, multiple sequence alignment; NDH-2, NADH dehydrogenase II; pfam10709, Protein family 10709; PDB, Protein Data Bank; SEC–MALS, size-exclusion chromatography with multiangle light scattering; TCEP, Tris(2-carboxyethyl) phosphine.

References

1. Rensing, C., and McDevitt, S. F. (2013) The copper metallome in prokaryotic cells. In: Banci, L., ed. *Metallomics and the Cell*, Springer, Dordrecht: 417–450
2. Argüello, J. M., Raimunda, D., and Padilla-Benavides, T. (2013) Mechanisms of copper homeostasis in bacteria. *Front. Cell. Infect. Microbiol.* **3**, 14
3. Ladomersky, E., and Petris, M. J. (2015) Copper tolerance and virulence in bacteria. *Metallomics* **7**, 957–964
4. Macomber, L., and Imlay, J. A. (2009) The iron-sulfur clusters of dehydratases are primary intracellular targets of copper toxicity. *Proc. Natl. Acad. Sci. U. S. A.* **106**, 8344–8349
5. Brancaccio, D., Gallo, A., Piccioli, M., Novellino, E., Ciofi-Baffoni, S., and Banci, L. (2017) [4Fe-4S] cluster assembly in mitochondria and its impairment by copper. *J. Am. Chem. Soc.* **139**, 719–730
6. Giachino, A., and Waldron, K. J. (2020) Copper tolerance in bacteria requires the activation of multiple accessory pathways. *Mol. Microbiol.* **114**, 377–390
7. Outten, F. W., Huffman, D. L., Hale, J. A., and O'Halloran, T. V. (2001) The independent cue and cus systems confer copper tolerance during aerobic and anaerobic growth in *Escherichia coli*. *J. Biol. Chem.* **276**, 30670–30677
8. Rensing, C., Fan, B., Sharma, R., Mitra, B., and Rosen, B. P. (2000) CopA: An *Escherichia coli* Cu(I)-translocating P-type ATPase. *Proc. Natl. Acad. Sci. U. S. A.* **97**, 652–656
9. Outten, F. W., Outten, C. E., Hale, J., and O'Halloran, T. V. (2000) Transcriptional activation of an *Escherichia coli* copper efflux regulon by the chromosomal MerR homologue, cueR. *J. Biol. Chem.* **275**, 31024–31029
10. Kim, E. H., Nies, D. H., McEvoy, M. M., and Rensing, C. (2011) Switch or funnel: How RND-type transport systems control periplasmic metal homeostasis. *J. Bacteriol.* **193**, 2381–2387
11. Chacón, K. N., Mealman, T. D., McEvoy, M. M., and Blackburn, N. J. (2014) Tracking metal ions through a Cu/Ag efflux pump assigns the functional roles of the periplasmic proteins. *Proc. Natl. Acad. Sci. U. S. A.* **111**, 15373–15378
12. Affandi, T., and McEvoy, M. M. (2019) Mechanism of metal ion-induced activation of a two-component sensor kinase. *Biochem. J.* **476**, 115–135
13. Cooksey, D. A. (1994) Molecular mechanisms of copper resistance and accumulation in bacteria. *FEMS Microbiol. Rev.* **14**, 381–386
14. Brown, N. L., Barrett, S. R., Camakaris, J., Lee, B. T. O., and Rouch, D. A. (1995) Molecular genetics and transport analysis of the copper-resistance determinant (pco) from *Escherichia coli* plasmid pRJ1004. *Mol. Microbiol.* **17**, 1153–1166
15. Cha, J. S., and Cooksey, D. A. (1993) Copper hypersensitivity and uptake in *Pseudomonas syringae* containing cloned components of the copper resistance operon. *Appl. Environ. Microbiol.* **59**, 1671–1674
16. Djoko, K. Y., Xiao, Z., and Wedd, A. G. (2008) Copper resistance in *E. coli*: The multicopper oxidase PcoA catalyzes oxidation of copper(I) in Cu^{I}-Cu^{II}-PcoC. *ChemBioChem* **9**, 1579–1582

17. Lawton, T. J., Kenney, G. E., Hurley, J. D., and Rosenzweig, A. C. (2016) The CopC family: Structural and bioinformatic insights into a diverse group of periplasmic copper binding proteins. *Biochemistry* **55**, 2278–2290
18. Mellano, M. A., and Cooksey, D. A. (1988) Nucleotide sequence and organization of copper resistance genes from *Pseudomonas syringae* pv. tomato. *J. Bacteriol.* **170**, 2879–2883
19. Zhang, X. X., and Rainey, P. B. (2008) Regulation of copper homeostasis in *Pseudomonas fluorescens* SBW25. *Environ. Microbiol.* **10**, 3284–3294
20. Chillappagari, S., Miethke, M., Trip, H., Kuipers, O. P., and Marahiel, M. A. (2009) Copper acquisition is mediated by YcnJ and regulated by YcnK and CsoR in *Bacillus subtilis*. *J. Bacteriol.* **191**, 2362–2370
21. Hirooka, K., Edahiro, T., Kimura, K., and Fujita, Y. (2012) Direct and indirect regulation of the *ycnKJI* operon involved in copper uptake through two transcriptional repressors, YcnK and CsoR, in *Bacillus subtilis*. *J. Bacteriol.* **194**, 5675–5687
22. Kenney, G. E., Sadek, M., and Rosenzweig, A. C. (2016) Copper-responsive gene expression in the methanotroph *Methylosinus trichosporium* OB3b. *Metallomics* **8**, 931–940
23. González-Guerrero, M., Raimunda, D., Cheng, X., and Argüello, J. M. (2010) Distinct functional roles of homologous Cu^+ efflux ATPases in *Pseudomonas aeruginosa*. *Mol. Microbiol.* **78**, 1246–1258
24. Ekici, S., Turkarslan, S., Pawlik, G., Dancis, A., Baliga, N. S., Koch, H. G., and Daldal, F. (2014) Intracytoplasmic copper homeostasis controls cytochrome *c* oxidase production. *mBio* **5**, e01055-13
25. Hassani, B. K., Astier, C., Nitschke, W., and Ouchane, S. (2010) CtpA, a copper-translocating P-type ATPase involved in the biogenesis of multiple copper-requiring enzymes. *J. Biol. Chem.* **285**, 19330–19337
26. Osman, D., Patterson, C. J., Bailey, K., Fisher, K., Robinson, N. J., Rigby, S. E., and Cavet, J. S. (2013) The copper supply pathway to a *Salmonella* Cu, Zn-superoxide dismutase (SodCII) involves P_{1B}-type ATPase copper efflux and periplasmic CueP. *Mol. Microbiol.* **87**, 466–477
27. Myers, K. S., Yan, H., Ong, I. M., Chung, D., Liang, K., Tran, F., Keleş, S., Landick, R., and Kiley, P. J. (2013) Genome-scale analysis of *Escherichia coli* FNR reveals complex features of transcription factor binding. *PLoS Genet.* **9**, e1003565
28. Rouch, D. A., and Brown, N. L. (1997) Copper-inducible transcriptional regulation at two promoters in the *Escherichia coli* copper resistance determinant *pco*. *Microbiology* **143**, 1191–1202
29. Boysen, A., Møller-Jensen, J., Kallipolitis, B., Valentin-Hansen, P., and Overgaard, M. (2010) Translational regulation of gene expression by an anaerobically induced small non-coding RNA in *Escherichia coli*. *J. Biol. Chem.* **285**, 10690–10702
30. Durand, S., and Storz, G. (2010) Reprogramming of anaerobic metabolism by the FnrS small RNA. *Mol. Microbiol.* **75**, 1215–1231
31. Rensing, C., and Grass, G. (2003) *Escherichia coli* mechanisms of copper homeostasis in a changing environment. *FEMS Microbiol. Rev.* **27**, 197–213
32. Zhang, L., Koay, M., Maher, M. J., Xiao, Z., and Wedd, A. G. (2006) Intermolecular transfer of copper ions from the CopC protein of *Pseudomonas syringae*. Crystal structures of fully loaded Cu(I)Cu(II) forms. *J. Am. Chem. Soc.* **128**, 5834–5850
33. Arnesano, F., Banci, L., Bertini, I., and Thompsett, A. R. (2002) Solution structure of CopC: A cupredoxin-like protein involved in copper homeostasis. *Structure* **10**, 1337–1347
34. Arnesano, F., Banci, L., Bertini, I., Mangani, S., and Thompsett, A. R. (2003) A redox switch in CopC: An intriguing copper trafficking protein that binds copper(I) and copper(II) at different sites. *Proc. Natl. Acad. Sci. U. S. A.* **100**, 3814–3819
35. Osipov, E. M., Lilina, A. V., Tsallagov, S. I., Safonova, T. N., Sorokin, D. Y., Tikhonova, T. V., and Popov, V. O. (2018) Structure of the flavocytochrome *c* sulfide dehydrogenase associated with the copper-binding protein CopC from the haloalkaliphilic sulfur-oxidizing bacterium *Thioalkalivibrio paradoxus* ARh 1. *Acta Crystallogr. D Struct. Biol.* **74**, 632–642
36. Udagedara, S. R., Wijekoon, C. J. K., Xiao, Z., Wedd, A. G., and Maher, M. J. (2019) The crystal structure of the CopC protein from *Pseudomonas fluorescens* reveals amended classifications for the CopC protein family. *J. Inorg. Biochem.* **195**, 194–200
37. Pozzi, R., Coles, M., Linke, D., Kulik, A., Nega, M., Wohlleben, W., and Stegmann, E. (2016) Distinct mechanisms contribute to immunity in the lantibiotic NAI-107 producer strain *Microbispora* ATCC PTA-5024. *Environ. Microbiol.* **18**, 118–132
38. Juncker, A. S., Willenbrock, H., Von Heijne, G., Brunak, S., Nielsen, H., and Krogh, A. (2003) Prediction of lipoprotein signal peptides in Gram-negative bacteria. *Protein Sci.* **12**, 1652–1662
39. Rahman, O., Cummings, S. P., Harrington, D. J., and Sutcliffe, I. C. (2008) Methods for the bioinformatic identification of bacterial lipoproteins encoded in the genomes of Gram-positive bacteria. *World J. Microb. Biot.* **24**, 2377–2382
40. ElGamacy, M., Riss, M., Zhu, H., Truffault, V., and Coles, M. (2019) Mapping local conformational landscapes of proteins in solution. *Structure* **27**, 853–865
41. Giner-Lamia, J., Lopez-Maury, L., and Florencio, F. J. (2015) CopM is a novel copper-binding protein involved in copper resistance in *Synechocystis* sp PCC 6803. *Microbiologyopen* **4**, 167–185
42. Pontel, L. B., and Soncini, F. C. (2009) Alternative periplasmic copper-resistance mechanisms in Gram negative bacteria. *Mol. Microbiol.* **73**, 212–225
43. Lewinson, O., Lee, A. T., and Rees, D. C. (2009) A P-type ATPase importer that discriminates between essential and toxic transition metals. *Proc. Natl. Acad. Sci. U. S. A.* **106**, 4677–4682
44. Grass, G., and Rensing, C. (2001) Genes involved in copper homeostasis in *E. coli*. *J. Bacteriol.* **183**, 2145–2147
45. Trasnea, P. I., Utz, M., Khalfaoui-Hassani, B., Lagies, S., Daldal, F., and Koch, H. G. (2016) Cooperation between two periplasmic copper chaperones is required for full activity of the cbb_3 -type cytochrome *c* oxidase and copper homeostasis in *Rhodobacter capsulatus*. *Mol. Microbiol.* **100**, 345–361
46. Rapisarda, V. A., Chehín, R. N., De Las Rivas, J., Rodríguez-Montelongo, L., Farías, R. N., and Massa, E. M. (2002) Evidence for Cu(I)-thiolate ligation and prediction of a putative copper-binding site in the *Escherichia coli* NADH dehydrogenase-2. *Arch. Biochem. Biophys.* **405**, 87–94
47. Volentini, S. I., Farías, R. N., Rodríguez-Montelongo, L., and Rapisarda, V. A. (2011) Cu(II)-reduction by *Escherichia coli* cells is dependent on respiratory chain components. *Biometals* **24**, 827–835
48. Rodríguez-Montelongo, L., Volentini, S. I., Farías, R. N., Massa, E. M., and Rapisarda, V. A. (2006) The Cu(II)-reductase NADH dehydrogenase-2 of *Escherichia coli* improves the bacterial growth in extreme copper concentrations and increases the resistance to the damage caused by copper and hydroperoxide. *Arch. Biochem. Biophys.* **451**, 1–7
49. Melo, A. M., Bandeiras, T. M., and Teixeira, M. (2004) New insights into type II NAD(P)H:quinone oxidoreductases. *Microbiol. Mol. Biol. Rev.* **68**, 603–616
50. Rapisarda, V. A., Montelongo, L. R., Farías, R. N., and Massa, E. M. (1999) Characterization of an NADH-linked cupric reductase activity from the *Escherichia coli* respiratory chain. *Arch. Biochem. Biophys.* **370**, 143–150
51. Hao, Z., Lou, H., Zhu, R., Zhu, J., Zhang, D., Zhao, B. S., Zeng, S., Chen, X., Chan, J., He, C., and Chen, P. R. (2014) The multiple antibiotic resistance regulator MarR is a copper sensor in *Escherichia coli*. *Nat. Chem. Biol.* **10**, 21–28
52. Djoko, K. Y., Xiao, Z., Huffman, D. L., and Wedd, A. G. (2007) Conserved mechanism of copper binding and transfer. A comparison of the copper-resistance proteins PcoC from *Escherichia coli* and CopC from *Pseudomonas syringae*. *Inorg. Chem.* **46**, 4560–4568
53. Grass, G., and Rensing, C. (2001) CueO is a multicopper oxidase that confers copper tolerance in *Escherichia coli*. *Biochem. Biophys. Res. Commun.* **286**, 902–908
54. Franke, S., Grass, G., Rensing, C., and Nies, D. H. (2003) Molecular analysis of the copper-transporting efflux system CusCFBA of *Escherichia coli*. *J. .Bacteriol.* **185**, 3804–3812
55. Tottey, S., Rondet, S. A. M., Borrelly, G. P. M., Robinson, P. J., Rich, P. R., and Robinson, N. J. (2002) A copper metallochaperone for photosynthesis

and respiration reveals metal-specific targets, interaction with an importer, and alternative sites for copper acquisition. *J. Biol. Chem.* **277**, 5490–5497
56. Prior, S. D., and Dalton, H. (1985) The effect of copper ions on membrane content and methane monooxygenase activity in methanol-grown cells of *Methylococcus capsulatus* (Bath). *J. Gen. Microbiol.* **131**, 155–163
57. Pomowski, A., Zumft, W. G., Kroneck, P. M., and Einsle, O. (2011) N_2O binding at a [4Cu:2S] copper-sulphur cluster in nitrous oxide reductase. *Nature* **477**, 234–237
58. Söding, J., Biegert, A., and Lupas, A. N. (2005) The HHpred interactive server for protein homology detection and structure prediction. *Nucleic Acids Res.* **33**, W244–W248
59. Finn, R. D., Clements, J., and Eddy, S. R. (2011) HMMER web server: Interactive sequence similarity searching. *Nucleic Acids Res.* **39**, W29–W37
60. Katoh, K., and Standley, D. M. (2014) MAFFT: Iterative refinement and additional methods. *Methods Mol. Biol.* **1079**, 131–146
61. Steinegger, M., Meier, M., Mirdita, M., Vöhringer, H., Haunsberger, S. J., and Söding, J. (2019) HH-suite3 for fast remote homology detection and deep protein annotation. *BMC Bioinformatics* **20**, 473
62. Sali, A., and Blundell, T. L. (1993) Comparative protein modelling by satisfaction of spatial restraints. *J. Mol. Biol.* **234**, 779–815
63. Lindahl, E., Hess, B., and van der Spoel, D. (2001) GROMACS 3.0: A package for molecular simulation and trajectory analysis. *J. Mol. Model.* **7**, 306–317
64. Lindorff-Larsen, K., Piana, S., Palmo, K., Maragakis, P., Klepeis, J. L., Dror, R. O., and Shaw, D. E. (2010) Improved side-chain torsion potentials for the Amber ff99SB protein force field. *Proteins* **78**, 1950–1958
65. Ashkenazy, H., Abadi, S., Martz, E., Chay, O., Mayrose, I., Pupko, T., and Ben-Tal, N. (2016) ConSurf 2016: An improved methodology to estimate and visualize evolutionary conservation in macromolecules. *Nucleic Acids Res.* **44**, W344–W350
66. Baba, T., Ara, T., Hasegawa, M., Takai, Y., Okumura, Y., Baba, M., Datsenko, K. A., Tomita, M., Wanner, B. L., and Mori, H. (2006) Construction of *Escherichia coli* K-12 in-frame, single-gene knockout mutants: The Keio collection. *Mol. Syst. Biol.* **2**, 2006.0008
67. Zallot, R., Oberg, N., and Gerlt, J. A. (2019) The EFI web resource for genomic enzymology tools: Leveraging protein, genome, and metagenome databases to discover novel enzymes and metabolic pathways. *Biochemistry* **58**, 4169–4182
68. Potter, S. C., Luciani, A., Eddy, S. R., Park, Y., Lopez, R., and Finn, R. D. (2018) HMMER web server: 2018 update. *Nucleic Acids Res.* **46**, W200–w204
69. Waterhouse, A. M., Procter, J. B., Martin, D. M. A., Clamp, M., and Barton, G. J. (2009) Jalview Version 2-a multiple sequence alignment editor and analysis workbench. *Bioinformatics* **25**, 1189–1191
70. Shannon, P., Markiel, A., Ozier, O., Baliga, N. S., Wang, J. T., Ramage, D., Amin, N., Schwikowski, B., and Ideker, T. (2003) Cytoscape: A software environment for integrated models of biomolecular interaction networks. *Genome Res.* **13**, 2498–2504
71. Kabsch, W. (2010) Integration, scaling, space-group assignment and post-refinement. *Acta Cryst.* **D66**, 133–144
72. Terwilliger, T. C., Adams, P. D., Read, R. J., McCoy, A. J., Moriarty, N. W., Grosse-Kunstleve, R. W., Afonine, P. V., Zwart, P. H., and Hung, L. W. (2009) Decision-making in structure solution using Bayesian estimates of map quality: The PHENIX AutoSol wizard. *Acta Crystallogr. D Biol. Crystallogr.* **65**, 582–601
73. Terwilliger, T. C., Grosse-Kunstleve, R. W., Afonine, P. V., Moriarty, N. W., Zwart, P. H., Hung, L. W., Read, R. J., and Adams, P. D. (2008) Iterative model building, structure refinement and density modification with the PHENIX AutoBuild wizard. *Acta Crystallogr. D Biol. Crystallogr.* **64**, 61–69
74. Emsley, P., and Cowtan, K. (2004) Coot: Model-building tools for molecular graphics. *Acta Cryst.* **D60**, 2126–2132
75. Liebschner, D., Afonine, P. V., Baker, M. L., Bunkóczi, G., Chen, V. B., Croll, T. I., Hintze, B., Hung, L. W., Jain, S., McCoy, A. J., Moriarty, N. W., Oeffner, R. D., Poon, B. K., Prisant, M. G., Read, R. J., *et al.* (2019) Macromolecular structure determination using X-rays, neutrons and electrons: Recent developments in phenix. *Acta Crystallogr. D Struct. Biol.* **75**, 861–877
76. Williams, C. J., Headd, J. J., Moriarty, N. W., Prisant, M. G., Videau, L. L., Deis, L. N., Verma, V., Keedy, D. A., Hintze, B. J., Chen, V. B., Jain, S., Lewis, S. M., Arendall, W. B., 3rd, Snoeyink, J., Adams, P. D., *et al.* (2018) MolProbity: More and better reference data for improved all-atom structure validation. *Protein Sci.* **27**, 293–315
77. Sharan, S. K., Thomason, L. C., Kuznetsov, S. G., and Court, D. L. (2009) Recombineering: A homologous recombination-based method of genetic engineering. *Nat. Protoc.* **4**, 206–223